ASSEMBLY OF MOUSE HEPATITIS VIRUS STRAIN JHM

Andrew Massalski, Marion Coulter-Mackie and Samuel Dales

Cytobiology Group, Department of Microbiology and Immunology, University of Western Ontario
London, Ontario N6A 5C1 Canada

INTRODUCTION

Coronaviruses have been characterized as a separate group (26), predominantly based on the morphology of their unique, massive peplomers and single stranded $^{+}$RNA genome (22). Electron microscopic studies on different members of this group revealed that assembly occurs in the cytoplasm, where progeny are formed by a budding process from membranes of either the endoplasmic reticulum and/or cytoplasmic vacuoles (9). The budding process has been described in some detail in the case of avian infectious bronchitis virus, the human agent, 229E (2), and other isolates (3, 7, 10, 16, 18, 23, 24, 25, 29, 30). Despite the preponderance of data favouring budding as the assembly mechanism some reservations have been made about the significance of this process (11, 27). The present electron microscopic study was undertaken to ascertain at high resolution the nature of coronavirus assembly, with particular attention to the incompletely characterized nucleocapsid.

MATERIAL AND METHODS

Cells and Viruses

Mouse 17Cl-1 cells of the passage are derivative of 3T3 BALB/c cells and were kindly provided by Dr. L.S. Sturman (Division of Laboratories and Research, N.Y. State Department of Health, Albany, N.Y.). They are routinely maintained in Eagle's minimal essential medium (MEM) supplemented with 10% heat-inactivated fetal bovine serum (Microbiological Associates), sodium bicarbonate (2 g/l), penicillin (100 u/ml) and streptomycin (100 mg/l) in a humidified atmosphere with 5% CO_2. The JHM strain of murine coronavirus was

V. ter Meulen et al. (eds.), *Biochemistry and Biology of Coronaviruses*

obtained from the American Type Culture Collection (Rockville, Maryland).

Growth and JHM Infection of Cells for EM

Cells were grown to monolayer in 30 mm plastic tissue culture dishes and infected with JHM at a multiplicity of 0.004 - 0.2 pfu/cell. After 1 hour adsorption at 32.5°, cultures were washed with phosphate buffered saline, overlaid with 2 ml MEM, and incubated at 32.5° for 24 or 48 hr prior to sampling. A range of multiplicities was employed in order to obtain samples representing various stages of infection at 24 and 48 hr, the two times chosen for sampling.

Electron Microscopy

Cell monolayers in which syncytia formation was evident were fixed in situ by flooding with 2% Glutaraldehyde in 0.05 M Phosphate buffer at pH 7.2 and postfixed with 1% OsO_4 according to our previous method (8). Following washing and dehydration in ethanol series, the cells were infiltrated with 1:1 mixture of absolute ethanol and Epon 812. The monolayers were finally covered with approximately 2-3 mm thick layer of Epon 812 and polymerized at 60°C for 24 hr. Small fragments of the hardened disks were cut out and mounted in orientations which permitted the monolayer to be sectioned both horizontally and vertically. Unsupported 200 mesh grids were used to collect sections, which were subsequently double-stained for 4 min with 5% Uranyl acetate in 50% Ethanol, followed by 3 mins with lead citrate solution (21). The specimens were examined in a Philips EM300 at an accelerating voltage of 60 or 80 KV.

RESULTS AND DISCUSSION

In order to facilitate sampling for examination of virus development by transmission electron microscopy, monolayers of Cl 17-1 cells were infected with JHM virus at multiplicities sufficiently low to initiate slow, progressive syncytiogenesis, described previously (14). The syncytia scattered throughout the monolayers are evident initially within 24 hr postinfection and become quite extensive by 48 hr. In order to preserve as faithfully as possible the structural relationship between sites of virus development and related cellular organelles as they may occur in the living state, fixation and embedding of attached cells were carried out in situ. This procedure facilitated a precise localization and selection of areas in the monolayer where syncytiogenesis was evident by light microscopy.

Examination of horizontally sectioned syncytia revealed presence of numerous vacuoles ranging in diameter from 150-160 nm

(Fig. 1). Absence of ribosomes on the cytoplasmic face of the vacuole membranes implies that these structures are derived from smooth endoplasmic reticulum (SER). Their random distribution, as ascertained by both vertical and horizontal sections implies that they occur throughout the cytoplasm. Occurrence of circular rather than flattened profiles of the sectioned vacuoles indicates that the SER becomes distended following infection. Virus assembly is confined to these vacuoles (Figs. 1 and 2), and has not been observed at either the plasma membrane or any other cellular surface. This is in agreement with other studies of the coronaviruses (22), but at variance with sites of assembly of enveloped viruses from the myxo-, paramyxo- and rhabdovirus groups (5, 20, 4, 12, 28).

An interpretation of the dynamic events during JHM virus assembly in the polykaryocytes was based upon a series of images ordered into a developmental sequence (Figs. 3-10). The most rudimentary stage was identified by presence of a short segment of dense material subjacent to the vacuolar membrane (Figs. 3-5). An associated unit membrane was clearly evident on the external surface (Figs. 3-5), and is presumed to represent the viral envelope covered by the peplomers (Figs. 9 and 10). Elongated structures, which in some images appeared to be tubular in nature, were organized on the cytoplasmic side of the modified vacuolar surface (Figs. 2-6). In the more advanced stages of budding the virus envelopes surrounded the elongated, internal component to a varying degree (Figs. 2 and 7-10). In favourable orientations the tubular nature of the internal component could be discerned (Figs. 7-8). These structures are highly reminiscent of the nucleoprotein helix of influenza virus (1). The external diameter of the coronavirus tubules is on the average 9.5 nm, ranging from 8.5 to 10.5 nm. These dimensions correspond to measurements made on the extruded coronavirus helical component evident by negative staining (13, 19), and a dense internal thread present within thinly sectioned infectious avian bronchitis virus (1). An internal component of a greater diameter has been recorded in one study (15). Our measurements also correspond to the diameter of the influenza virus nucleoprotein, measuring either 6-9 nm in sectioned virions (1) or 10-15 nm in whole mount preparations (5, 20). By contrast the diameter of the helical nucleocapsid of the paramyxoviruses, 15-19 nm in diameter is about double the width of the coronavirus tubular structure (4, 6, 12, 17). According to another recent interpretation the coronavirus nucleocapsid structure is described as a circular, dense, inner component, about 60 nm wide (10). Our new evidence, coupled with information obtained on disrupted negatively stained 229E virions (13, 15), and another representative of the group (19), indicates that the architecture of the coronaviruses simulates that of the myxo- and paramyxoviruses, although the coronaviruses unlike the other two groups, possess a single stranded RNA genome of the + sense. From this observation it may be

Figs. 1-10 Sections of infected Cl 17-1 cells sampled 48 hr after inoculation and perserved in situ to demonstrate assembly and distribution of virus progeny.

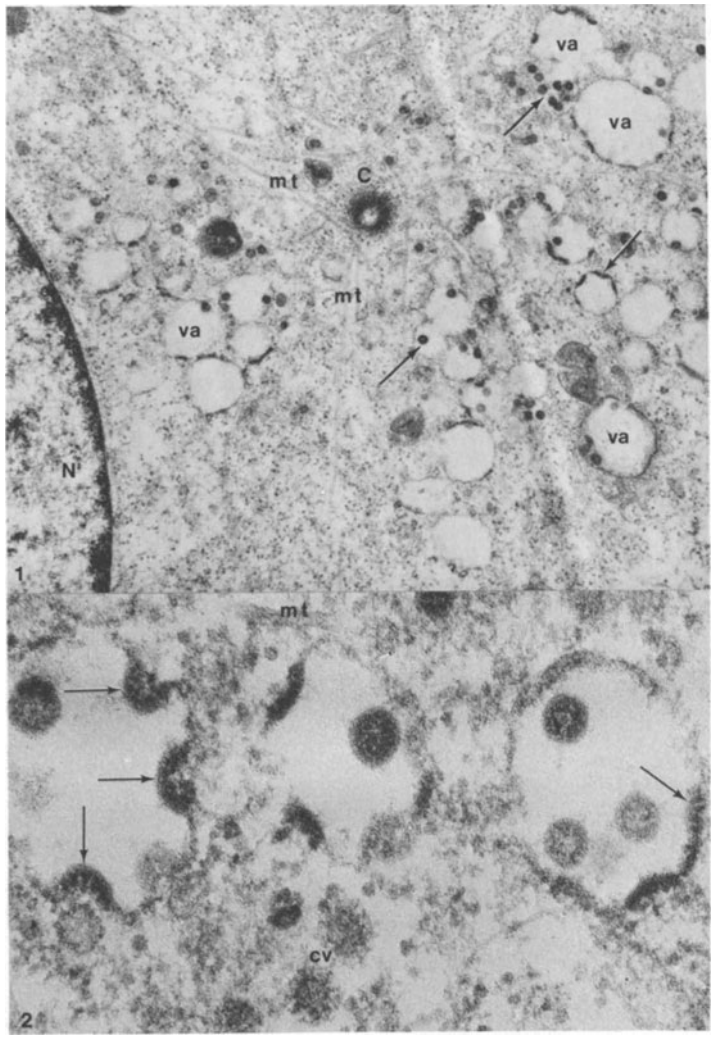

Fig. 1 Illustrates at lower magnification presence of cytoplasmic vacuoles (va) containing budding or free virus particles (arrows). C: centriole; mt: microtubules; N: nucleus. X 31,000.

Fig. 2 An example at higher resolution reveals stages of virus assembly at the membranes of vacuoles (arrows). mt: microtubule; cv: coated vesicle. X 138,000.

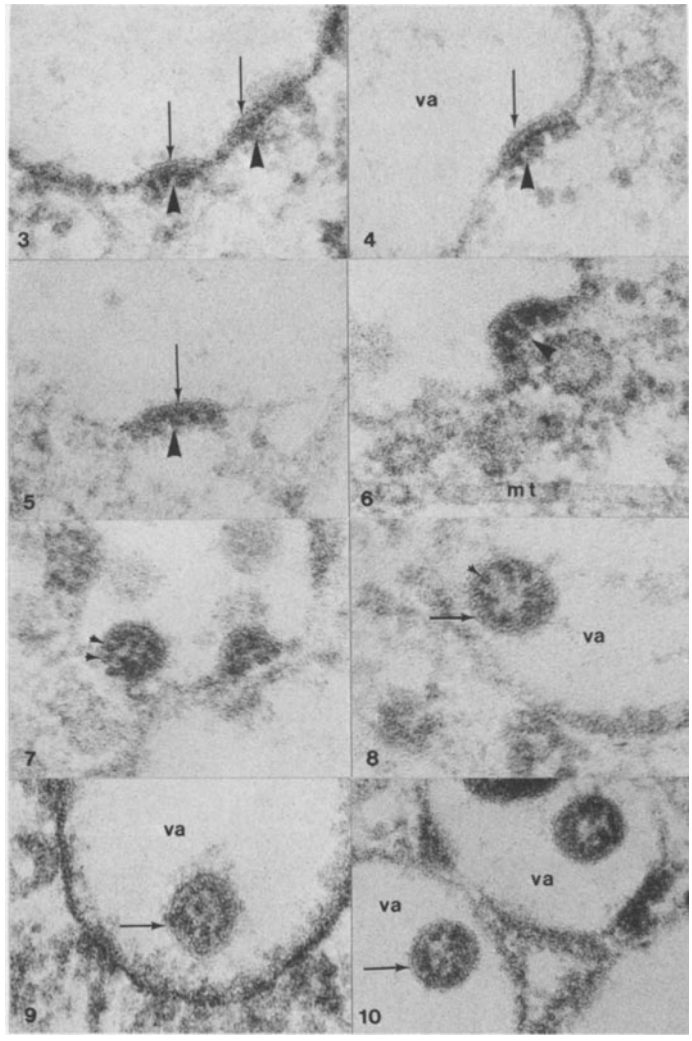

Figs. 3-10 Selected areas at high resolution demonstrating virus budding at membranes of vacuoles. The series represents reconstruction of the presumed assembly sequence. The virus envelope, either in continuity with the vacuole membrane (Figs. 3-7), or enclosing virions (Figs. 8-10), is indicated by arrows. The nucleocapsids indicated by arrowheads are evident as tubular structure in either the longitudinal aspect (Figs. 6 and 8), or in cross section (Fig. 7), during the formative stages (Figs. 3-7) and in completed virions (Fig. 8). mt: microtubule; va: vacuole. Fig. 8 X 240,000; all others X 200,000.

concluded that polarity of the RNA genome and helical conformation of the nucleoprotein are not necessarily interrelated.

ACKNOWLEDGEMENTS

Supported by the Medical Research Council and Multiple Sclerosis Society of Canada.

REFERENCES

1. K. Apostolov, T.H. Flewett, and A.P. Kendal, Morphology of Influenza A,B,C and Infectious Bronchitis Virus (IBV) Virions and their Replication, in: "The Biology of large RNA viruses", R.D. Barry and B.W.J. Mahy, ed., Academic Press, London-New York (1970).
2. W.B. Becker, K. McIntosh, J.H. Dees, and R.M. Chanock, Morphogenesis of avian infectious bronchitis virus and a related human virus (strain 229E), J. Virol. 1:1019 (1967).
3. D. Chasey, and D.J. Alexander, Morphogenesis of avian infectious bronchitis virus in primary chick kidney cells, Arch. Virol. 52:101 (1976).
4. P.W. Choppin, and W. Stoeckenius, The morphology of SV5 virus, Virol. 23:195 (1964).
5. R.W. Compans, J. Content, and P.H. Duesberg, Structure of the ribonucleoprotein of influenza virus, J. Virol. 10:795 (1972).
6. R.W. Compans, K.V. Holmes, S. Dales, and P.W. Choppin, An electron microscopic study of moderate and virulent virus-cell interactions of the Parainfluenza Virus SV5, Virol. 30:411 (1966).
7. C.H. Cunningham, M.P. Spring, and K. Nazerian, Replication of avian infectious bronchitis virus in African green monkey kidney cell line VERO, J. gen. Virol. 16:432 (1972).
8. S. Dales, and H. Hanafusa, Penetration and intracellular release of the genomes of Avian RNA tumor viruses, Virol. 50:440 (1972).
9. J.F. David-Ferreira, and R.A. Manaker, An electron microscope study of the development of a mouse hepatitis virus in tissue culture cells, J. Cell Biol. 24:57 (1965).
10. H.J.A. Fleury, R.D. Sheppard, M.B. Bornstein, and C.S. Raine, Further ultrastructural observations of virus morphogenesis and myelin pathology in JHM virus encephalomyelitis. Neuropath. App. Neurobiol. 6:165 (1980).
11. D. Hamre, D.A. Kindig, and J. Mann, Growth and intracellular development of a new respiratory virus, J. Virol. 1:810 (1967).
12. R.W. Horne, A.P. Waterson, P. Wildy, and A.E. Farnham, The structure and composition of the Myxoviruses. 1. Electron

microscope studies of the structure of Myxovirus particles by negative staining techniques, Virol. 11:79 (1960).
13. D.A. Kennedy, and C.M. Johnson-Lussenberg, Isolation and morphology of the internal component of human coronavirus, strain 229E, Intervirol. 6:197 (1976).
14. A. Lucas, W. Flintoff, R. Anderson, D. Percy, M. Coulter, and S. Dales, In vivo and in vitro models of demyelinating diseases: I. Tropism of the JHM strain of murine hepatitis virus for cells of glial origin, Cell 12: 553 (1977).
15. M.R. Macnaughton, H.A. Davies, and M.V. Nermut, Ribonucleoprotein like structures from coronavirus particles, J. Gen. Virol. 39:545 (1978).
16. K. Nazerian, and C.H. Cunningham, Morphogenesis of avian infectious bronchitis virus in chicken embryo fibroblasts, J. gen. Virol. 3:469 (1968).
17. E.C.J. Norrby, and P. Magnusson, Some morphological characteristics of the internal component of Measles virus, Arch. ges. Virusforsch 17:443 (1964).
18. L.S. Oshiro, J.H. Schieble, and E.H. Lennette, Electron microscopic studies of coronavirus, J. gen. Virol. 12:161 (1971).
19. D.H. Pocock, and D.J. Garwes, The polypeptides of hemagglutinating encephalomyelitis virus and isolated subviral particles, J. gen. Virol. 37:487 (1977).
20. M.W. Pons, I.T. Schulze, and G.K. Hirst, Isolation and characterization of the ribonucleoprotein of influenza virus, Virol. 39:250 (1969).
21. E.S. Reynolds, The use of lead citrate at high pH as an electron-opaque strain in electron microscopy, J. Cell Biol. 17:208 (1963).
22. J.A. Robb, and C.W. Bond, Coronaviridae, in: "Comprehensive Virology", H. Fraenkel-Conrat and R. Wagner, ed., Plenum, New York (1979).
23. J.A. Robb, and C.W. Bond, Pathogenic murine coronaviruses. 1. Characterization of biological behavior in vitro and virus specific intracellular RNA of strongly neurotropic JHMV and weakly neurotropic A59V viruses, Virol. 94:352 (1979).
24. J.A. Robb, C.W. Bond, and J.L. Leibowitz, Pathogenic murine coronaviruses. 111. Biological and biochemical characterization of temperature-sensitive mutants of JHMV, Virol. 94:385 (1979).
25. B.H. Ruebner, T. Hirano, and R.J. Slusser, Electron microscopy of the hepatocellular and Kupffer cell lesions of mouse hepatitis with particular reference to the effect of cortisone, Amer. J. Path. 51:163 (1967).
26. D.A.J. Tyrrell, J.D. Almeida, C.H. Cunningham, W.R. Dowdle, M.S. Hoestad, K. McIntosh, M. Tajima, Y.L. Zakstelskaya, B.C. Easterday, A. Kapikian, and R.W. Bingham, Coronaviridae, Intervirol. 5:76 (1975).

27. P.K. Uppal, and H.P. Chu, An electron microscope study of the trachea of the fowl infected with avian infectious bronchitis virus, J. med. Microbiol. 3:643 (1970).
28. R.R. Wagner, Reproduction of Rhabdoviruses, in: "Comprehensive Virology", H. Fraenkel-Conrat and R. Wagner, eds., Plenum, New York (1975).
29. K. Watanabe, Electron microscopic studies of experimental viral hepatitis in mice. 1. Virus particles and their relationship to hepatocytes and Kupffer cells, J. Electron Micro. 18:158 (1969).
30. K.H. Witte, M. Tajima, and B.C. Easterday, Morphologic characteristics and nucleic acid type of transmissible gastroenteritis virus of pigs, Arch. ges. Virusforsch. 23:53 (1968).